Unraveling the Innermost Regions of Transitional Disks with the Keck Interferometer

Jorg-Uwe Pott[1]

W. M. Keck Observatory, California Association for Research in Astronomy, 65-1120 Mamalahoa Hwy, Kamuela, HI 96743
Division of Astronomy, University of California, Los Angeles, CA 90095
Max-Planck-Institut für Astronomie, Königstuhl 17, D-69117 Heidelberg, Germany

Marshall D. Perrin

Division of Astronomy, University of California, Los Angeles, CA 90095

Elise Furlan

Jet Propulsion Laboratory, Caltech, Mail Stop 264-767, 4800 Oak Grove Drive, Pasadena, CA 91109

Stanimir Metchev

Department of Physics and Astronomy, State University of New York, Stony Brook, NY 11794-3800

Andrea M. Ghez

Division of Astronomy, University of California, Los Angeles, CA 90095

Tom M. Herbst

Max-Planck-Institut für Astronomie, Königstuhl 17, D-69117 Heidelberg, Germany

ABSTRACT

We have studied the innermost regions of several nearby, young "transitional" disks, which are characterized by a significant depletion of optically thick dust close to the star. Using near-infrared long baseline interferometry, we test the possibility that stellar binarity might explain the characteristic near-to-mid infrared SEDs of theses stars by clearing away dust from the inner disks. With the Keck Interferometer, we obtain milliarcsecond angular resolution in the K-band for five such transitional disks in the Taurus/Auriga star-forming region. The

observed visibilities exclude nearly the entire parameter range of binary companions from 2.5 - 30 mas (0.35 - 4 AU). This binary range could dynamically cause inner hole sizes of several AU in the optically thick dust distribution, a scale estimated by typical SED model fits. A few binary models, oriented along the Keck baseline, are less constrained and cannot be ruled out for companions fainter than about 10 % of the primary's luminosity at 2 μm. But assuming a random distribution of binary position angles over our sample, we can exclude binarity on a statistical basis as the typical origin for the clearing of inner dust in transitional disks. Instead, we find indications for emission from hot circumstellar material on 0.1 AU scales in all five of our targets. This supports the notion that some transitional disks have radial gaps in their optically thick material, which could be an indication for planet formation in the habitable zone ($\sim$ a few AU) of a protoplanetary disk.

Subject headings: planetary systems: protoplanetary disks — Keck: Interferometer — stars: pre–main sequence — circumstellar matter — stars: individual (DM Tau, GM Aur, LkCa 15, UX Tau A, RY Tau)

1. Introduction

Circumstellar disks are a natural outcome of the star-formation process: when a molecular cloud core collapses, it gives rise to a central star surrounded by a rotating circumstellar disk, which transports material towards the star. Over time, the disk material dissipates through accretion onto the central star and the formation of planets. At an age of $\sim$ 5 Myr, about 90% of disks have already dispersed, and within 10 Myr of their formation, almost all pre-main-sequence stars are diskless (e.g. Sicilia-Aguilar et al. 2006). It is now well established that such disks commonly give rise to planetary systems, but the details of this process remain unclear. Theory predicts that disks evolve from the inside out: dust grain growth is expected to occur faster in the inner disk than in the outer disk (e.g. van Boekel et al. 2004; Dullemond & Dominik 2005), higher densities favor planet formation in the inner disk (Boss et al. 2002), and photoevaporation by the central star will cause the inner disk to dissipate first (Clarke et al. 2001).

In fact, a small number of so-called "transitional disks" have been observed, which show a strong mid-infrared excess revealing the presence of dust but lack near-IR excess emission, suggesting that their inner disk regions have already been cleared out to a radius of a few AU (Skrutskie et al. 1990; Meyer et al. 1997; Stassun et al. 2001; D'Alessio et al. 2005; Calvet et al. 2005; McCabe et al. 2006; Furlan et al. 2006; Lada et al. 2006; Muzerolle et al. 2006;

Espaillat et al. 2007a; Brown et al. 2007). Therefore, these disks might be in the process of dispersing, potentially due to the influence of newly formed planets. The variety of observing constraints give a complex picture. Some disk data favour an inner *hole*, which refers to a true depletion of the inner optically thick dust. In general, it is assumed that dust (traced by the IR continuum) and gas (traced by emission lines) are well mixed in primordial disks. But gas has been found in inner disk regions void of optically thick dust. In some cases, a disk *gap* is present, when optically thick dust close to the stellar photosphere, as traced by 2 μm excess emission, is separated by a gap from the outer, cooler, optically thick dust disk, which is detected at far-infrared and (sub-)mm wavelengths (Espaillat et al. 2008; Brown et al. 2008; Salyk et al. 2009, and references therein). The detailed morphology of the inner disk is unclear. The NIR excess could derive from a small, ring-like optically thick dust region very close to the star, or rather from a wider distribution of optically thin dust extending from the inner boundary of the cooler disk towards the star (e.g. Espaillat et al. 2008). In the following, we use the term *transitional disk* for all young stellar disks with a clear dust excess at wavelengths longer than about 8 μm, and little or no dust excess at some or all wavelengths shorter than 8 μm.

In nearby star-forming regions, typically a few percent of pre-main-sequence stars are found to harbor transitional disks (Taurus-Auriga: Furlan et al. (2006), NGC 2068/71: Flaherty & Muzerolle (2008)). These numbers can increase significantly up to a few tens of percent, depending on the exact definition of transitional disks, in particular if and what type of inner disk emission is included (Furlan et al. 2009, submitted). Given the age of $\sim 1-2$ Myr for these regions, a transitional disk fraction of a few percent implies a relatively short time scale of $\sim 10^5$ years for the disk clearing stage. This calculation holds, if the observed partial lack of dust is attributed to the evolution of the stellar disk, namely the beginning of its clearing, and if all disks are assumed to pass this inner clearing phase. High resolution imaging and spectroscopic observations, in conjunction with disk models, suggest that gaps are also common in partially cleared disk. Further observational constraints are needed to understand the location of the inner dust emission regions, to get a more complete picture of the disk evolution.

The disk clearing picture is further complicated by the fact that most young stars are found in multiple systems: the companion star fraction in young, nearby star-forming regions is about 50% in the 15-1800 AU separation range and $\sim$ 20% at separations less than 10 AU (Ghez et al. 1993, 1997; Leinert et al. 1993; Simon et al. 1995). These binaries affect the simple interpretation of apparent transitional disk systems in two ways; first, unresolved infrared companions can create an excess that appears almost identical to that of a transitional disk (Duchêne et al. 2003), and, second, binary companions can perturb a circumstellar disk (e.g. see the discussion for DI Tau in Meyer et al. 1997). A circumbinary

disk is typically truncated at an inner radius of about 2-3 times the semimajor axis of the binary. Artymowicz & Lubow (1994) investigated the gravitational impact of a central binary on a geometrically thin, non-self gravitating circumbinary disk, and found that the semi-major axis of the central binary is about half the inner disk edge-radius. The detailed relation between binary separation and disk hole size depends on the binary's eccentricity. This implies that an inner disk hole of 10 AU could be caused by a companion orbiting the primary at about 3-5 AU. To call such a circumbinary disk *transitional*, would be misleading, since circumbinary disks can be dynamically stable and longer-lasting. Such a binary-disk configuration would mimic the appearance of a short-lived transitional disk, although the disk clearing has not yet begun. Photoevaporation however is expected to similarly clear out the inner disk and produce holes rather than gaps in the dust distribution. Direct imaging constraints from high-resolution measurements at 2 μm are definitely needed to better understand the stellar and disk properties inside of transitional disks.

For CoKu Tau/4, the transitional disk system with the largest fully cleared-out inner disk hole, recent work near the limit of AO resolution indicates that this hole is actually caused by a newly discovered binary companion (Ireland & Kraus 2008), and there is no need to invoke planet formation as the disk clearing mechanism. Might binarity be responsible for the cleared-out appearance of other "transitional" disks? While the companion star fraction typically decreases towards smaller separations (less than a few AU), the census of close companions is far from complete. Ireland & Kraus (2008) report no detection of companions with mass ratio > 0.1 outside of 4 AU for other transitional disks in Taurus, but cannot constrain closer companions. Melo (2003) suggest that YSOs in Ophiuchus have a companion fraction of at least 10% at the 0.8-4 AU separation scale. However, the short-period binary frequency appears to vary between different sites of star formation (Mathieu 1992; Melo 2003). Thus, it is not clear what fraction of transitional disks might be caused by truncation due to a stellar companion rather than other processes. Many of the other transitional disks typically have inferred inner disk edges smaller than that of CoKu Tau/4. With disk holes of the order of 10 AU or less, the only way to resolve the inner disk regions is by interferometric observations.

To assess the presence of close binary companions within other transitional disks, we used the Keck Interferometer (KI) in V^2 mode[1] to test for stellar multiplicity in 5 transitional disks in the nearby ($\sim$ 140 pc) Taurus-Auriga young star-forming region (Sect. 2). The nominal interferometric resolution of $\sim$ 5 mas and field of view of 50 mas offered in V^2 mode is well suited to resolve any companion stars from about 0.5 to 5 AU from the target primary

[1] V^2-mode measures the continuum squared visibility amplitude of the astronomical K'-band

stars. This angular resolution is a significant improvement over the resolution available with speckle interferometry and adaptive optics ($\sim$ 50 mas).

The method is sensitive to companions with orbital periods ranging from several months to several years, a regime that could also be probed by radial velocity surveys. Unfortunately, such surveys would take years to complete. Only one epoch of KI data is sufficient to probe a large binary parameter space, since the Earth's rotation of the KI baseline allows us to obtain visibilities at about 5 independent *spatial frequencies* (or *u,v*-points) per object per night. For some of our targets, we are able to combine our data with previous interferometric measurements; RY Tau: Akeson et al. (2005a), LkCa 15, GM Aur: Akeson et al. (2005b).

This article is organized as follows: we describe the target selection in Sect. 2. Observations and data reduction are reported in Sect. 3. The results are discussed in Sect. 4, and the conclusions of our experiment are given in Sect. 5

2. Target selection

Our sample consists of five low-mass pre-main sequence stars in the Taurus-Auriga star forming region showing mid-infrared dust excess characteristic of transitional disks: DM Tau, GM Aur, LkCa 15, UX Tau A, and RY Tau. These objects comprise the best-studied disks to date (i) with strong evidence from observations or SED-modelling that inner disk holes or gaps are present (D'Alessio et al. 2005; Calvet et al. 2005; Espaillat et al. 2007b, see Table 1) and (ii) for which no close binary companions are known (i.e., all but CoKu Tau/4). Our data probe binary separations of 2.5-30 mas (0.35-4 AU). This matches the inner disk region, which cannot be resolved by single telescope imaging of 8-10 m class telescopes, and which lies inside the colder optically thick dust disks, responsible for the MIR-excess of transitional disks.

Table 1 lists the stellar and disk properties of our targets and associated references. DM Tau is the only object in our sample with no detectable excess emission below 8 μm, but it is still accreting, traced by hydrogen emission lines. This suggests that at least gas must exist in the innermost disk, feeding the accretion. GM Aur has a hole of 24 AU, which is partially filled with optically thin dust. Both LkCa 15 and UX Tau A seem to have gaps between optically thick inner and outer disk regions; in addition, LkCa 15 also has some optically thin dust in the gap. RY Tau was recently identified in Furlan et al. (2009, submitted) as a possible transitional disk with a gap, in part due to its somewhat similar SED shape to LkCa 15. On the other hand, RY Tau has an earlier spectral type than the rest of the sample, and therefore its disk structure could be different.

Table 1: Stellar properties of the targets, and disk properties from previously published models.

	DM Tau[a]	GM Aur[a]	LkCa 15[b]	UX Tau A[b]	RY Tau[c]
M_* ($M_\odot$)	0.65	1.2	1.1	1.5	2.0
R_* ($R_\odot$)	1.2	1.5	1.7	2.0	3.6
T_* (K)	3720	4730	4350	4900	5945 [d]
L_* ($L_\odot$)	0.25	1.03	0.96	2.18	12.8
$\dot{M}$ ($M_\odot$ yr^{-1})	$2.0{\cdot}10^{-9}$	$1.0{\cdot}10^{-8}$	$2.4{\cdot}10^{-9}$	$9.6{\cdot}10^{-9}$	$2.5{\cdot}10^{-7}$
Spectral type	M1	K5	K5	K2	G1 [d]
A_V	0.5	1.2	1.2	1.3	2.1
K_s mag. [e]	9.5	8.3	8.2	7.5	5.4
Inclination (deg)	40	55	42	60	25
$R_{\text{inner disk}}$ (AU)	3	< 5	0.12..0.15	0.16..0.18	0.2..0.3
$K_{\text{inner disk}}/K_{\text{total}}$	0.0	0.12	0.23	0.32	0.73

[a]Calvet et al. (2005)

[b]Espaillat et al. (2007b)

[c]Akeson et al. (2005a)

[d]Calvet et al. (2004)

[e]Skrutskie et al. (2006)

Note. — The fractional K-band excess $K_{\text{inner disk}}/K_{\text{total}}$ is the flux ratio of disk to total light at K band, as inferred from previous models. Those models were based on spatially unresolved photometry, and, in the case of RY Tau, also on interferometric data from PTI. Note that Akeson et al. (2005b) report a fractional K-band excess of 0.43 for LkCa 15 from pure photometry fits. Here we use the 0.23 from Espaillat et al. (2007b) however, since they included NIR spectra in the fit, which clearly show and quantify the hot dust emission.

3. Observations and data reduction

The Keck Interferometer (KI) atop Mauna Kea combines the light of the two 10-meter Keck telescopes and has a baseline of 85-meters, oriented 38° east of north (Colavita et al. 2004; Wizinowich et al. 2004). We used the KI in the V^2 continuum mode. All data shown here are from the white-light channel of the beam combiner, which illuminates one pixel with the full K'-band (2-2.4 μm) to maximize sensitivity. This also provides the greatest sensitivity to small changes in the visibility over the parallactic angle range of the observations.

The observations were conducted on the nights of Mar. 17, and Dec. 15, 2008 (UT). Details of the observations appear in Table 2. KI data are provided to the observer in a semi-raw state. The technical calibration (such as detector bias corrections), and some averaging has been applied by a pipeline reduction. The result are raw fringe contrast (visibility) measurements, which still need to be calibrated for the so-called system visibility (the visibility transfer function), and the ratio correction, which corrects for systematic flux biases between the telescopes. Both the system visibility and the flux ratios proved to be very stable over the two nights, indicating a reliable data calibration. Due to these stable conditions and good seeing, we did not follow up each target with a calibrator immediately, but rather alternated two targets with one visibility calibrator measurement. We used a couple of different calibrator sources throughout the night to enable cross calibration, and to match the targets in brightness within $\pm$ 1 mag to account for the known flux-dependence of the KI system visibility (Akeson et al. 2007).

The calibrators were selected using either the getCal planning tool [2] or browsing SIMBAD directly within a radius of $\sim 15°$ around the science targets. We only used stars from the Hipparcos and Tycho catalogs to assure high coordinate precision. To ensure that all calibrator stars are unresolved with respect to the projected baseline, their photospheric diameters were estimated by fitting black-body SEDs to published photometry using NExScI's fbol routine (Table 3). The fitted black-body model was compared in particular to the photometry at wavelengths longer than 2 μm to check for dust excess that would be indicative of extended structure.

Our data reduction followed the standard procedures developed and suggested by the NExScI team, and we made ample use of their wb/nbCalib-software suite and the respective documentation. In particular, we used the time-windowing option to calculate the average

[2]Distributed by the NASA Exoplant Science Institute (NExScI): `http://nexsciweb.ipac.caltech.edu/gcWeb/gcWeb.jsp`

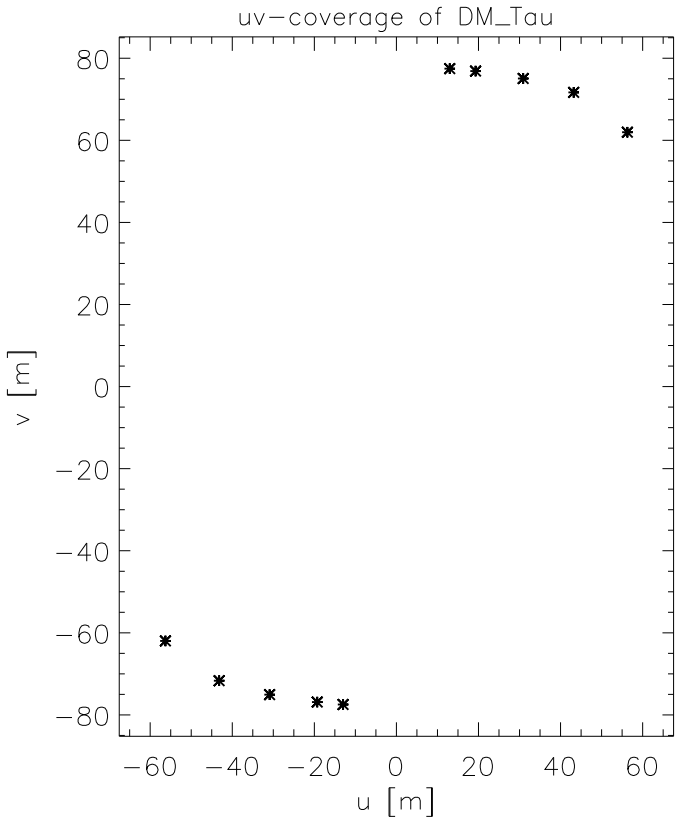

Fig. 1.— u,v-coverage of our KI observations of DM Tau. A significant u,v-coverage is necessary to probe a wide range of binary parameters. This u,v-coverage is typical for the other targets, since all have similar declinations as DM Tau. Note that each measurement creates two symmetric points in the u,v-plane.

Table 2: Observing log.

Target	date (UT)	H.A. [a]	u, v [b]	proj. B [b]	calibrators	V^2
		[hr]	[m]	[m, deg(EofN)]	[from Tab 3]	[calib.]
DM Tau	Mar.17,2008	3.3	(16.7, 77.1)	(78.9, 12.2)	1,2	0.91
	Mar.17,2008	3.4	(15.3, 77.3)	(78.8, 11.2)	1,2	0.91
	Dec.15,2008	-1.2	(56.3, 62.0)	(83.7, 42.2)	6,7	0.90
	Dec.15,2008	1.1	(43.2, 71.7)	(83.7, 31.1)	6,7	0.90
	Dec.15,2008	2.2	(30.9, 75.1)	(81.2, 22.4)	6,7	0.88
	Dec.15,2008	3.1	(19.3, 76.9)	(79.3, 14.1)	6,7	0.90
	Dec.15,2008	3.5	(13.0, 77.5)	(78.6, 9.5)	6,7	0.89
GM Aur	Mar.17,2008	2.6	(25.7, 80.2)	(84.2, 17.8)	1,2	0.95
	Dec.15,2008	-0.2	(52.7, 65.0)	(83.7, 39.0)	6,7	0.93
	Dec.15,2008	1.7	(36.9, 76.4)	(84.8, 25.8)	6,7	0.95
	Dec.15,2008	3.4	(14.2, 82.4)	(83.6, 9.8)	6,7	0.96
LkCa 15	Mar.17,2008	3.7	(10.9, 79.8)	(80.5, 7.8)	1,2	0.93
	Dec.15,2008	-1.0	(55.9, 62.2)	(83.6, 41.9)	6,7	0.91
	Dec.15,2008	1.5	(39.0, 74.2)	(83.8, 27.7)	6,7	0.91
	Dec.15,2008	2.6	(26.3, 77.7)	(82.0, 18.7)	6,7	0.91
	Dec.15,2008	3.3	(16.3, 79.3)	(81.0, 11.6)	6,7	0.91
UX Tau A	Dec.15,2008	-1.3	(56.4, 61.7)	(83.6, 42.4)	3,4,5	0.96
	Dec.15,2008	0.9	(45.3, 70.8)	(84.1, 32.6)	3,4,5	0.97
	Dec.15,2008	1.8	(35.7, 74.0)	(82.2, 25.8)	3,4,5	0.97
	Dec.15,2008	3.0	(20.3, 76.8)	(79.4, 14.8)	3,4,5	0.96
RY Tau	Mar.17,2008	2.6	(25.6, 79.8)	(83.8, 17.8)	1,2 [c]	0.30
	Dec.15,2008,	1.5	(39.4, 75.1)	(84.8, 27.7)	3,4,5	0.27
	Dec.15,2008	2.7	(24.4, 80.1)	(83.7, 16.9)	3,4,5	0.28

[a] hour angle

[b] the u, v-coordinates, given here in meters, are the baseline length (B) projected onto the line of sight. u points East, v points North. They are equivalent to polar values of the projected baseline, given in the next column in meters, and degrees East of North (compare to the u, v-coverage plot in Fig. 1). Note that the spatial frequency, inversely related to the interferometric resolution, is given by B/λ, the ratio of the variable baseline projection and the fixed observing wavelength (2.2 μm in our case).

[c] Note that these calibrators are, unlike during the Dec08 observations, significantly fainter than RY Tau, which can increase the systematic error of the visibility calibration by a few percent for the KI. Without a bright calibrator measurement during that night, we cannot quantify this increased calibration uncertainty for that particular night, but since the raw visibility, i.e. the system transfer function, decreases with flux, this measurement appears to be very consistent with the other data (cf. Fig. 2)

Table 3: Properties of the interferometric calibrator stars used for calibration of the instrumental transfer function during data reduction.

#	Calibrator	$V/H/K$	Spec. Type [a]	Ang. diameter (mas) [b]
1	HD283798[c]	9.5/8.1/8.0	G2V	0.11 ± 0.01
2	HD283886	9.9/8.6/8.4	G2V	0.08 ± 0.01
3	HD21379	6.3/6.3/6.3	A0V	0.12 ± 0.01
4	HD254236	8.8/6.5/6.3	K2III	0.34 ± 0.13
5	HD41076	6.1/6.1/6.1	A0V	0.13 ± 0.01
6	HD250388	10.7/8.9/8.8	K0	0.09 ± 0.01
7	HD283934	10.6/9.0/9.0	G5V	0.07 ± 0.01

[a] from SIMBAD

[b] bolometric diameter fit from the NEXSCI getCal tool.

[c] since this star is a pre-main sequence star, extra care is needed when using it as an interferometric calibrator due to possible photometric and diameter variability as well as extended NIR flux; however, it appeared unresolved in our observations, as well as in those of Akeson et al. (2005b)

Note. — Calibrator stellar diameters significantly smaller than 0.5 mas, are unresolved by the KI. The statistical errors given here for the bolometric diameter fit to a black body likely underestimate systematic errors of the NIR diameter of stars, but even 0.2 mas uncertainties in the diameter would not change the visibility calibration.

instrument transfer function or system visibility. The individual transfer functions as given by each calibrator measurement are defined as the ratio of the measured raw (squared) visibility to the respective ideal uniform disk (squared) visibility [3]. The calibration averaging scheme calculates a time and location dependent system transfer function on the basis of the relevant calibrator measurements within a time window of plus or minus two hours around the target. We use the time-weighting default option, which assumes that the calibration variance doubles within an hour from the time of the target measurement, thus giving half the maximum weight to a calibrator measurement if it is taken one hour apart from the target observation.

The closer the calibrator measurement matches the target observation in space and time, the stronger is its weight in the calculation of the average transfer function. This approach potentially minimizes the effect of a single bad calibration measurement on the data calibration, in contrast to using only the two calibrators immediately taken before and after the science measurement. This calculation of an average transfer function, based on all calibrator measurements, is particularly suitable for nights with stable observing conditions. Finally the raw data are divided by the transfer function to calculated the calibrated visibilities.

We use the standard deviation of the raw measurements as a first estimate of the uncertainties of each data point. The resulting statistical visibility uncertainties of the individual measurements are ~ 0.01 in most cases, smaller than the canonical value of 0.03 (see the NExScI KI support websites), which includes margin for systematics such as slightly different observing conditions and Strehl between the calibrator and science measurements. The calibrated visibility measurements appear in Table 2. Although the observing conditions were very good and stable throughout the night, and the calibration uncertainty seems to be slightly better than the canonical value, we assume the canonical $\delta V^2 = 0.03$ for the analysis in this paper, because we might have missed systematic biases due to a slightly sparser than usual[4] time-sampling of the system visibility. Since our goal was to detect visibility changes of 0.2 over the observed range in hour angles, our conclusions do not depend on the precise uncertainty adopted. Higher observing efficiency (i.e. time sampling) of the targets is more critical for our project than highest precision, to sample as large a range of binary parameters as possible. Still, the stable conditions and good visibility precision helped us to achieve the sensitivity to detect circumstellar material on scales as small as 1 milliarcsecond.

---

[3]following the measurement principles of the KI, the measurement is linear in the squared visibility modulus

[4]To get the highest precision, it is recommended to bracket a science object with two calibrator measurements at similar flux levels.

Fig. 1 shows the u,v-plane coverage of DM Tau. This is typical for the whole sample of targets.

4. Results

The calibrated visibilities appear in Fig. 2, plotted as a function of the hour angle and the projected baseline length. Since we show broad band visibilities, observed at a fixed central wavelength of about 2.2 μm, the projected baseline length scales the interferometric resolution (λ/B) and the spatial frequencies (B/λ) directly for all data shown. We added previously published KI data points for GM Aur and LkCa 15. For RY Tau, we also included in our analysis visibility measurements from a previous observation with the Palomar Testbed Interferometer (PTI, Akeson et al. 2005a). Due to the different baselines of the PTI measurements, in particular different position angles at similar baseline lengths, we do not show those data together with our KI data in the Fig. 2 . They probe different spatial frequencies at the hour angles and baseline-lengths shown in the figure. The data in Fig. 2 are shown as the measured squared visibility amplitudes. (Recall that an unresolved object has a visibility amplitude of unity.) All of our targets are resolved, with mean calibrated visibilities ranging from 0.28 ± 0.03 for RY Tau to 0.96 ± 0.03 for UX Tau A.

A quick look at the data in Fig. 2 immediately rules out that our science targets are unresolved at 2 μm, since the visibilities of all targets are significantly below one (apart for the marginally resolved UX Tau A). Thus, we can test our visibility data for each target against two contrary scenarios:

1. the extended near-IR emission comes from a stellar companion. A binary, detectable by the interferometer, would suggest that the inner disk is mostly clear of dust. In the following section, we demonstrate that a large range of binary parameters in the range of dynamical interaction between the binary and the inner disk edge can be excluded on basis of our KI data.

2. As an alternative to the binary scenario, we evaluate a simple model of a disk gap, simulating the inner dust disk by a face-on circumstellar ring which contributes to the K-band flux.

This ring-model is a pragmatic approach, typical for the interpretation of small visibility datasets. The resulting ring diameter gives order-of-magnitude constraints on the location and extension of the observed emission.

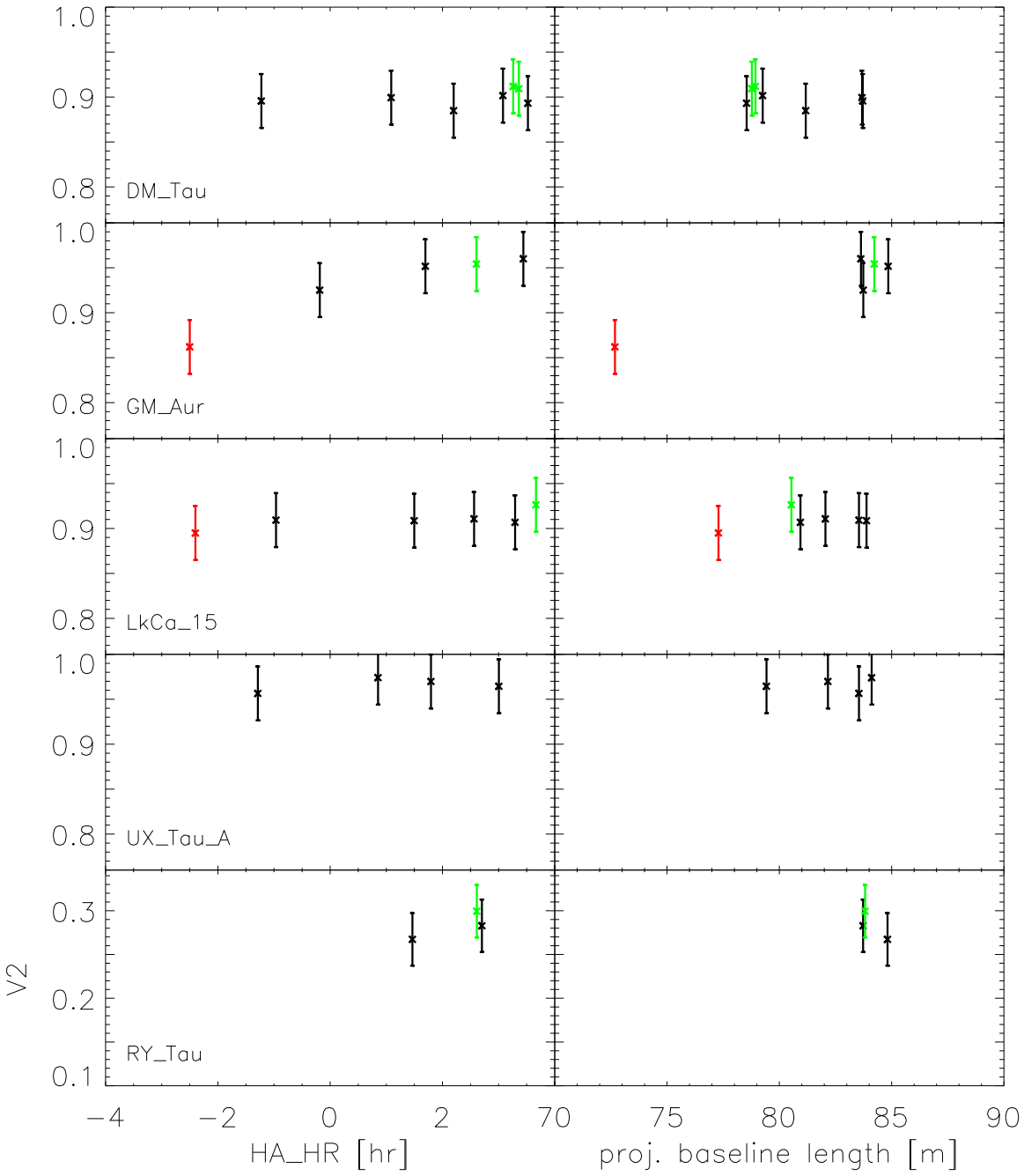

Fig. 2.— Calibrated V^2-data from our KI observation in March (green) and December (black) 2009, with 0.03 errors as discussed in the text. Note the different scaling of the ordinate axis. The red data points in the plots of GM Aur and LkCa 15 indicate the previously published KI data from Akeson et al. (2005b).

As seen in Fig. 2, we mostly sample a range of similar projected baseline lengths. Therefore, we cannot firmly conclude from the visibility data alone whether we resolve or over-resolve the dust emission. While resolved emission would result in decreasing visibilities with longer baselines, an over-resolved emission would show constant visibilities below unity. More information, for instance FR from the SED models, is needed to interpret the data best. Here, we aim at understanding at an order of magnitude level the physical location of the extended emission. Thus, details like scattered light contributions have not been considered in our analysis (Pinte et al. 2008).

4.1. Constraints on the presence of Binary Companions

Our overall approach is to test binary models against the observed visibilities, in order to rule out parts of the parameter space that are incompatible with the data. Due to the high maximum elevation of the Taurus-Auriga star forming region at Mauna Kea, the single baseline of the KI delivers sufficient u,v-coverage to probe a large range of binary parameters. We calculated theoretical visibilities for all position angles (PA) from 0-180° (the visibility sensitivity is point-symmetric), star-star separations ρ between 2.5 and 30 mas, and flux ratios (FR) between 1 and 0.05 times the brightness of the primary. We chose 180 linearly spaced steps for PA, while for ρ and FR we used 60, and 40 logarithmically spaced steps, respectively. This resembles Nyquist sampling of the parameters, given the KI's sensitivity to milliarcsecond-scale structures for *a priori* model fits. Thus, we examine about 43,000 possible binary configurations per star.

For each model the reduced χ^2 deviation to the data was calculated. Because the number of observed data points differ for each source (and thus the number of degrees of freedom for our model also varies) we calculate individually for each source the χ^2 level that corresponds to a 99.7% confidence level for the relevant number of degrees of freedom, based on the cumulative χ^2-distribution of random measurements. This level is arbitrarily chosen to match the 3 σ confidence level of a normal probability density function. Models whose (reduced) χ^2 exceeds this threshold have a probability of less than 0.3% to be consistent with the data and are rejected [5]. The thresholds are reported in Table 4.

The results are visualized in Fig. 3a &3b. In the left panels we show a 2.5 - 30 mas radius annulur patch of sky around each central star, the field of view (FOV) sampled by our observations. Note that this FOV refers to the fraction of the sky in which we can

[5]In general, statements in this paper about a model being 'consistent' or 'ruled out' by the data refer to this confidence level unless otherwise specified.

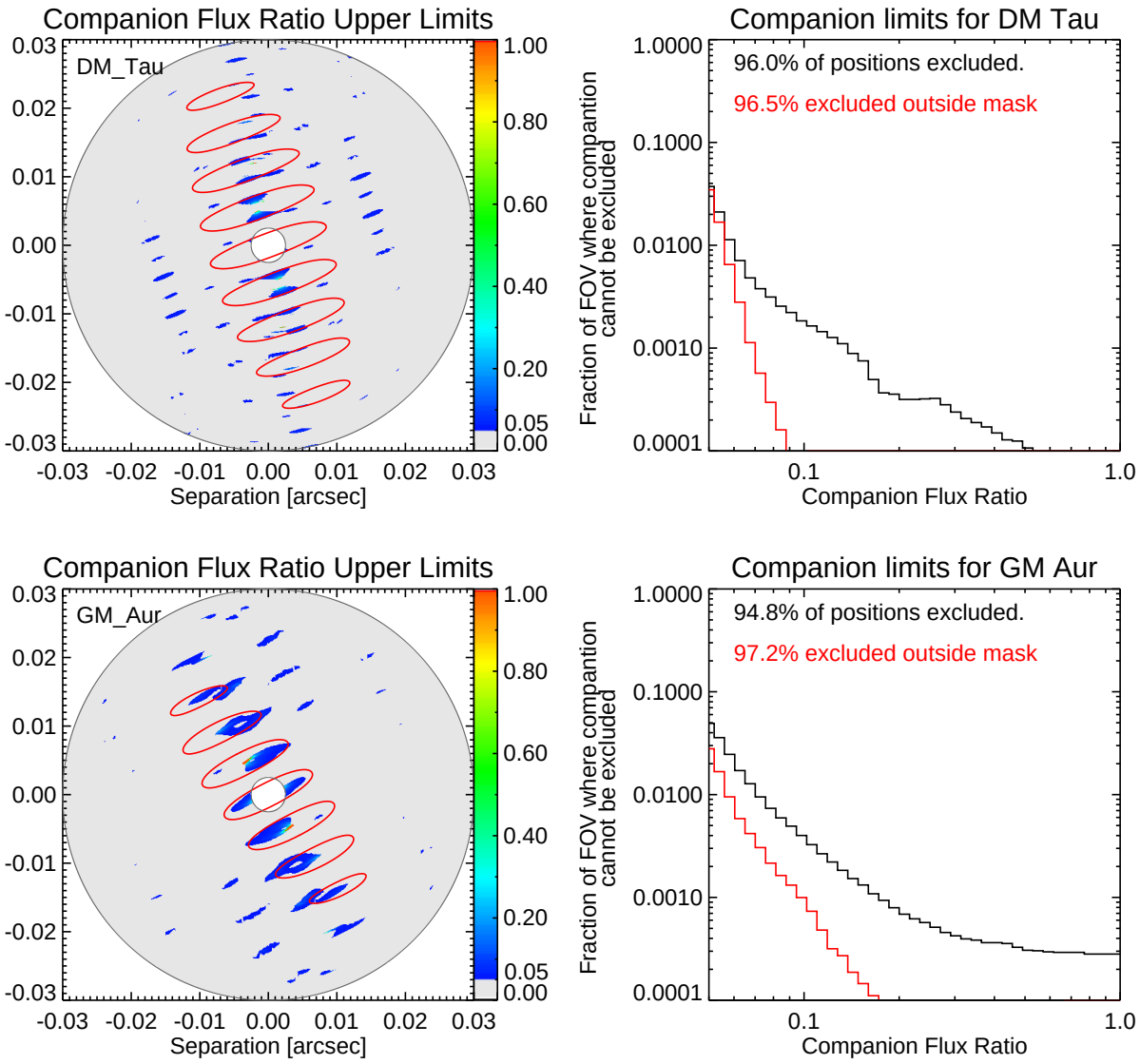

Fig. 3a.— Binary parameter exclusion plots for DM Tau, and GM Aur. The left figure shows for each position the brightest companion flux ratio that would be consistent with the observed visibilities. North is up, and East is to the left. An inner and outer ring (at 2.5 mas and 30 mas radius) show the FOV of our search. The red contours trace the interferometric PSF at a level equal to 1/3 of the PSF peak (the *mask* in the right panels). They indicate areas in which we have reduced binary FR sensitivity when observing visibilities close to unity (see text). The color bar (blue to orange) indicates the probed flux ratio range, and stops at $FR = 0.05$. The light grey region (labelled with zero at the color bar) indicates the area where no binary model with $1 \geq FR \geq 0.05$ fit the data. The right panel shows a normalized histogram of the limits in the left panel, as discussed in the text.

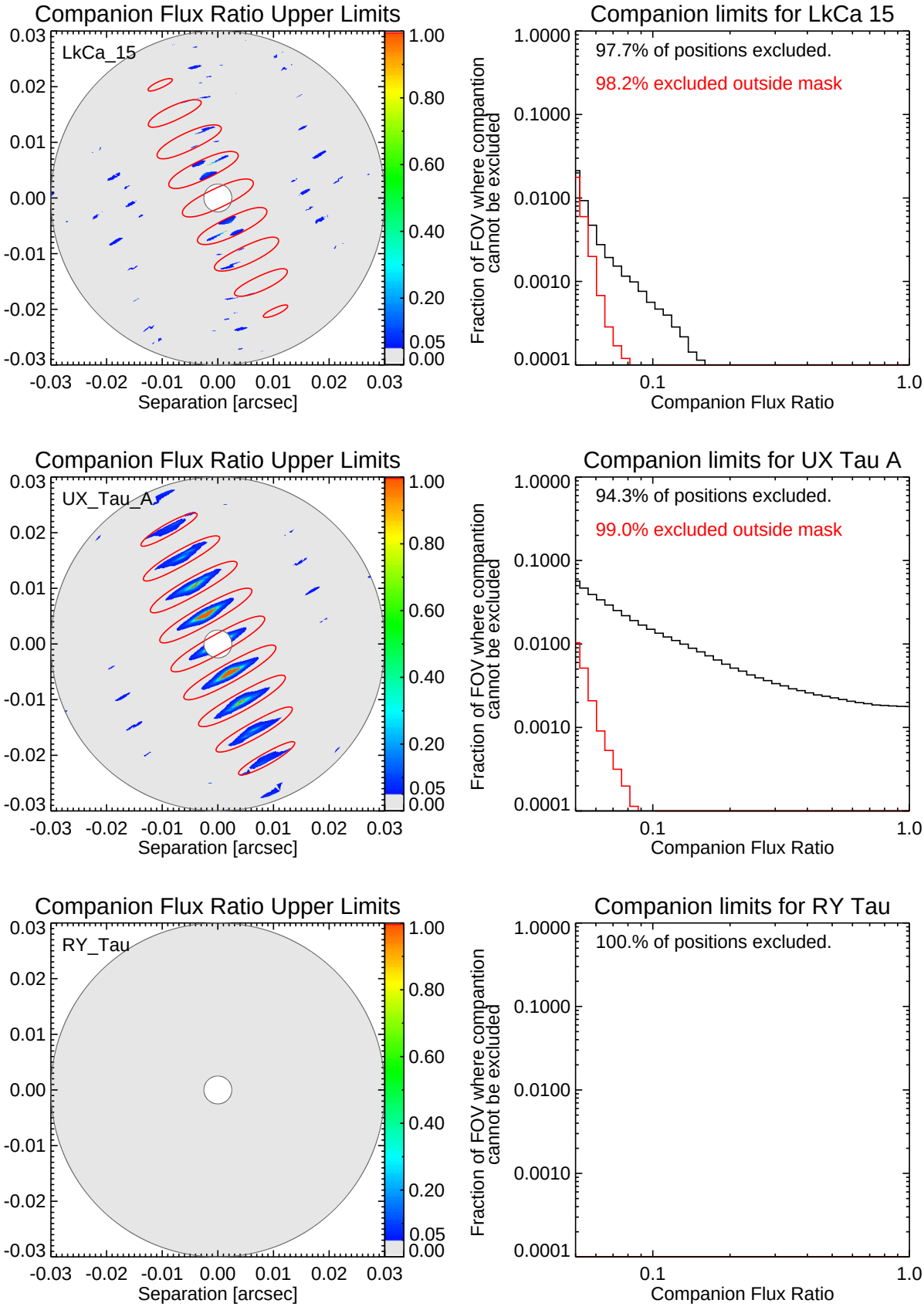

Fig. 3b.— Binary parameter exclusion plots for LkCa 15, UX Tau A, and RY Tau.

confidentially locate a binary companion. Such a analysis-specific FOV can differ from the general 50 mas FOV, given by the optical setup of the KI instrumentation. At each point in the annulus we plot color-coded the *brightest* companion flux ratio allowed for a companion at that location. For instance, the blue spots in the plot of DM Tau indicate, that we found, within the searched parameter space, binary solutions fitting the data, but only with a flux ratio smaller than 0.1.

For each target, the right panel in Fig. 3a&3b shows a normalized histogram of the sets of binary parameters that cannot be excluded with 99.7% confidence. The normalization creates uniform sky density of the parameter grid, so that the number of accepted solutions for a given flux ratio can be given as a fraction of the total FOV probed. The rejected fraction of the probed binary parameter range is given in the figure. Assuming equal probability for each set of parameters probed, this fraction gives the fraction of possible binaries that we can confidently rule out. These rejection fractions are also given in Table 4.

It appears that the solutions we find are not randomly spread over the FOV. In the following we argue that, most likely, they are artefacts of the sensitivity of the interferometer. To show that, we have overplotted in each of the left panels, for each of the four stars for which we only have KI data and for which we find some solutions, contour lines tracing the interferometric point spread function (iPSF) at 0.33 of its peak intensity (this iPSF is normalized to unity, and is the power spectrum of the interferometric, *projected* aperture during the observation). A single KI observation would show the characteristic grill-like iPSF of a two-element interferometer, multiplied with the single Keck PSF. As shown in the figure, the wings or side-lobes of our synthesized iPSF contribute a significant amount of power to the detected flux. Further these wings are roughly concentrated along the position of the Keck baseline. It is apparent that in regions where the iPSF is closer to unity, the rejection of binary parameter sets is less stringent. This results from the fact that we measure visibilities close to unity. If the companion is located in the wings of the iPSF, the measured visibility is high and the brightness distribution of the binary cannot be distinguished from a single point source (detailed detectability depends on the flux ratio). Note that the match between the binary solutions and the shape of the iPSF is best for UX Tau A, which shows the highest visibilities. If we decrease the FOV by the core of the iPSF (the red contours), the rejection fraction increases significantly as shown in the histograms. The contour level shown, 0.33, is chosen arbitrarily as a representative level, but of course there is iPSF structure at lower levels filling our entire field of view, and many of the regions with higher upper limits outside the contours are probably related to iPSF structure.

For all targets, companions with flux ratios greater than 1/20 of the primary are ruled out for the vast majority of separations and position angles. Companions with flux ratios

greater than 1/10 are typically only allowed for $< 0.5\%$ of the probed FOV. Note that a circle of the diameter of the KI resolution ($\lambda/B \sim 5$ mas) covers 0.8 % of the FOV. If we would observe a binary one can expect to find neighbouring solutions covering a continuous patch of the FOV, with a fractional size of order 0.5 % of the FOV. This is simply reflecting the angular resolution of the observations. Instead, we find very narrow regions of binary solutions, covering individually much less than this fraction. The are likely artefacts of the iPSF, in particular since these solutions are evenly spaced over the FOV, matching the spacing of the iPSF wings. If, as for our data, the remaining solution regions are spread over the FOV and *sum* up to $< 0.5\%$ (but do not reach this fraction individually), they are likely artefacts of the iPSF.

Outside of this inner working angle of 2.5 mas, it appears that the primary limit to our sensitivity is the iPSF structure, as just discussed. UX Tau A, which has visibilities closest to unity, thus has the loosest limits on possible companions. But the morphology of the iPSFs of DM Tau, GM Aur, LkCa 15, and UX Tau A are very similar, due to the similar sky coordinates of the targets. Since we can assume that no binary PA is preferred, it would be very unlikely that *all* of the four targets are in fact binaries oriented along the iPSF within the probed parameter range. Strictly speaking, we cannot exclude the shown binary solutions for the targets individually, but from a statistical point of view, it is unlikely that all four stars are binaries matching the insensitivities of an iPSF similar for all objects. For RY Tau, the fifth of our targets, all binary parameters of the probed parameter range, are excluded due to the significantly increased u,v-coverage after adding the PTI-data.

Combined across all five targets, binaries with flux ratios > 0.05 are ruled out for over 96.6% of the FOV, and flux ratios > 0.1 are ruled out for over 99.6%. If we exclude UX Tau A, those constraints rise to 97.1% and 99.8% respectively. The mass that these flux limits represent depends on both the luminosity of the primary and the assumed age of the system. Based on the PMS evolutionary tracks of Palla & Stahler (1999) and an age of 1 Myr, flux ratios of 0.1 would refer to companion masses of about 1/4 of the primary mass.

Thus it can be summarized that our observations

- exclude almost all of the probed binary parameter range, as given above, and
- reject stellar binarity as the dominant mechanism in creating a transitional disk appearance

4.2. Modeling the disk emission

For all targets but DM Tau, previous SED and high resolution studies concluded that significantly more than 5% of the K-band flux is not emitted by the central stellar object but rather is expected to come from some kind of circumstellar material (see also our individual target discussions below, and the references therein). As we have just established, we can exclude nearly all possible explanations which invoke a binary companion with flux ratio $FR > 0.05$. Furthermore, the fact that we resolve all targets with the interferometer indicates a significant K-band flux contribution from extended hot circumstellar matter. Thus it appears to be rather unlikely that the inner regions of these transitional disks are totally clear of dust. Instead, a gap must separate the innermost hot dust (visible at 2 μm) from the cooler dust which dominates the SED at wavelengths longer than about 8 μm. This correlates well with the fact that all our targets have been classified as *classical* T Tauri stars, with indications for ongoing mass accretion, which requires mass to be located close to the star.

If there *is* circumstellar dust radiating at 2 μm, the expected 3d-morphology is a ring at distances where the dust grain equilibrium temperature is comparable to sublimation temperatures of 1000-1500 K. Since our observations are limited to the K-band (at about 2 μm), we are not sensitive to cooler dust on scales of a few AU or larger.

The limited u,v-coverage inhibits a model-free interpretation of the visibility data, but without many additional assumptions, we can evaluate the following simple disk scenario, chosen to minimize the number of model parameters. We fit to our data a central point source plus a face-on, centro-symmetric, narrow ring, leaving only two degrees of freedom: the flux ratio between star and ring, and the ring radius. If, in fact, the simple model is reasonably close to the astrophysical reality, the fitted radii would represent the approximate, order of magnitude, location of the radiating material. Only if the emission morphology departed significantly from circular symmetry (jet-like, edge-on disk), would the radii derived here be less meaningful. Fitting more realistic *inclined* rings or disks would add at least two more parameters (position and inclination angles), and would essentially require measurements of an orthogonal baseline to obtain good constraints. Previous measurements do not show a very large inclination ($> 60°$) for any of the targets (Table 1), so in keeping with our small u,v-coverage, we do not explore this scenario. We did test a three-parameter model which lets the radial thickness of the bright ring also vary, but we found no significant improvement over the two-parameter model described here.

The results are shown in Fig. 4a-4b. For each target, the left panel shows the reduced χ^2 of the given model parameters; red contours indicate the χ^2 contour corresponding to 99.7% confidence, as described above. For GM Aur, LkCa 15, UX Tau A, and RY Tau, we have also

overplotted the disk-to-star flux ratio and disk inner radius estimates based on previous SED fits (Table 1). The horizontal dashed green lines in each plot represent a typical error ±5% for such photometry based NIR-excess estimation. Similarly, we over-plotted for DM Tau an upper limit of 5% $K_{\rm excess}/K_{\rm total}$. Calvet et al. (2005) find for GM Aur dust inside 5 AU, and the horizontal dashed lines represent the respective dust excess. But they cannot further constrain the location of this inner dust. Appropriately, no vertical line is given in the figure for this target.

The intersections of these lines with the regions of χ^2 close to unity give our fitted radii. Qualitatively the 'allowed' regions of the χ^2-plots in the left panel with χ^2 close to unity show two features: a diagonal feature for small ring radii where we truly have the angular resolution *and* sensitivity to resolve the ring, and a wavy horizontal feature at larger radii, where the ring is *over*-resolved. The flux ratio of this feature is connected to the average visibility level, and refers to how much of the total flux is over-resolved.

In the right panel of Fig. 4a&4b, we plot the minimum χ^2 per ring radius, from the parameter range within the SED-model estimated flux ratios (horizontal dashed lines in the left panels, also Table 1). The fact, that these minimum chi^2 are often significantly below unity, does not indicate that our used conservative V^2 uncertainty estimates including instrumental and observational systematics, are too large for the presented data. However, it indicates that these systematic biases do not necessarily change from data point to data point, and that the measurements are not completely independent at this accuracy level. We then derive our model radius for GM Aur, LkCa 15, and RY Tau as the radius of the minimum χ^2, for the disk-to-star flux ratios derived from the SEDs. For DM Tau and UX Tau A, we derive a lower, and a upper limit for the radius, respectively, as discussed below. Table 4 lists the best-fit model radius and χ^2 for each target, derived using the constraint of the disk-to-star flux ratios from SEDs. The vertical dashed lines in the right panels of Fig. 4a&4b show again the radii where dust emission is expected, as derived from SED models. There is a reasonable coincidence with the results from our visibility analysis for all targets.

Details for the individual targets are given in the following sections, but here we summarize the findings qualitatively.

- Because all sources are spatially resolved, even without SED models, our data require a minimum flux contribution from the inner disk. Since this is K-band flux, it cannot come from very large radii, where cooler dust resides (peaking at longer wavelengths). Thus, our data reject the scenario of a totally cleared inner disk. Scenarii for transitional disks, with some hot dust very close to the star and / or a transition zone with no or optically thin dust emission inside of the cooler, outer optically thick dust appear

consistent with the data.

- Our two-parameter star/ring model fits the data well within our confidence limits, but the radius is not well constrained by the imaging information from our KI data alone. Unambiguous model radii can be derived if we combine the visibilities with flux ratio constraints previously derived from SED models.

4.3. Discussion of Individual Targets

If not cited otherwise, the background information discussed in this section, in particular photometry and the Spitzer spectroscopy, is published or referenced in the survey articles of Furlan et al. (2006, 2009). All our five targets show the typical mid-IR excess at wavelengths longer than about 8 μm, and Spitzer IRS spectra reveal the 10 μm silicate emission feature, generated by optically thin dust in the surface layer of optically thick disks, or in gaps void of optically thick dust. The strength of the silicate feature varies between targets, and in particular UX Tau A shows very weak silicate emission, potentially due to larger grains in the inner disk from grain growth during disk evolution.

We discuss the stars below in increasing order of the expected disk contribution to the K-band flux as derived from SED-models.

4.3.1. DM Tau, expected $K_{\rm inner\,disk}/K_{\rm total}$: 0%

DM Tau does not show any significant emission excess at wavelengths shorter than 8 μm. Calvet et al. (2005) fit a typical dust disk model to the optical to mid-IR SED, including an IRS spectrum. They find no significant excess from dust closer than 3 AU to the star, although their model allows for small amounts of optically thin dust in the inner region. The upper limit for the optically thin dust mass is $7 \cdot 10^{-4}\,M_{\rm lunar}$. However, our visibility measurements clearly show that at least about 5% of the K-band flux is not emitted by the central star (see the horizontal feature of good solutions along the 5% line in Fig. 4a). Without an a priori star-to-inner disk flux ratio, we cannot completely constrain the average location of this inner dust from the star, as we do for the other targets. But, assuming a 5% upper limit for $K_{\rm excess}/K_{\rm total}$, we can *exclude* radii smaller than 0.2 AU, based on our ring-model.

Our measurement demonstrates that even a single calibrated KI data point is sensitive to a contribution from extended flux at the few percent level, a significant improvement over

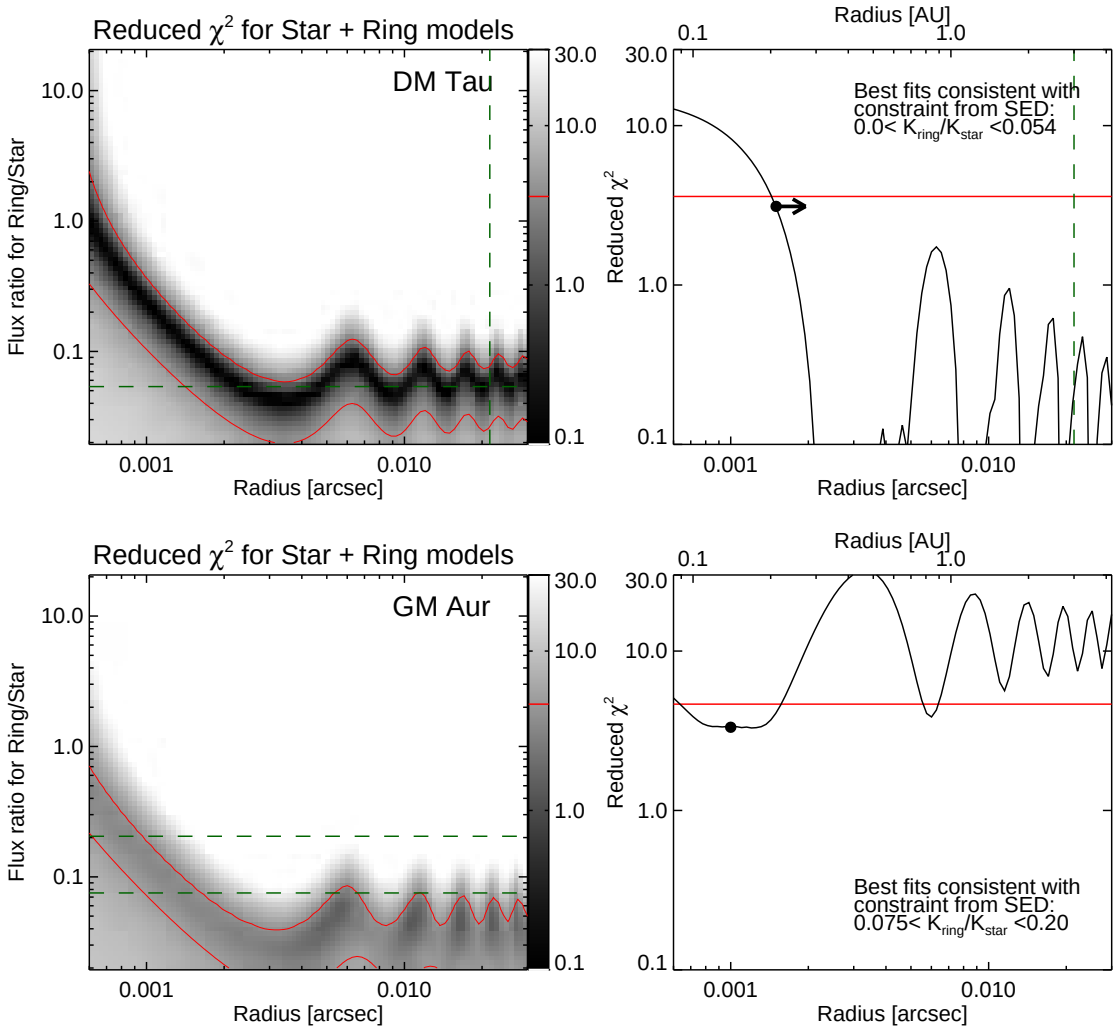

Fig. 4a.— Star plus ring fits to the interferometric data of DM Tau, and GM Aur. The left panels show the reduced χ^2 for each set of model parameters. Red lines in both panels trace the 99.7% confidence contours; models outside these contours do *not* fit our data, while models within these contours are possible based on the visibilities alone. The green dashed lines indicate the flux ratio and inner radius range inferred from previous SED fits (see Table 1). The color scaling for the left panel is indicated adjacent to the right panel. The right panel shows the minimum χ^2 per ring radius, estimated whithin the SED-derived flux ratio range. The ring diameter favored by our data is overplotted, and given in Table 4. Note that the arrow in the upper right plot of DM Tau, indicating the lower limit, matches the 1.5 mas given in the Table. The slight discrepancy to the 99.7 % level, the formal rejection criterion, is due to rounding.

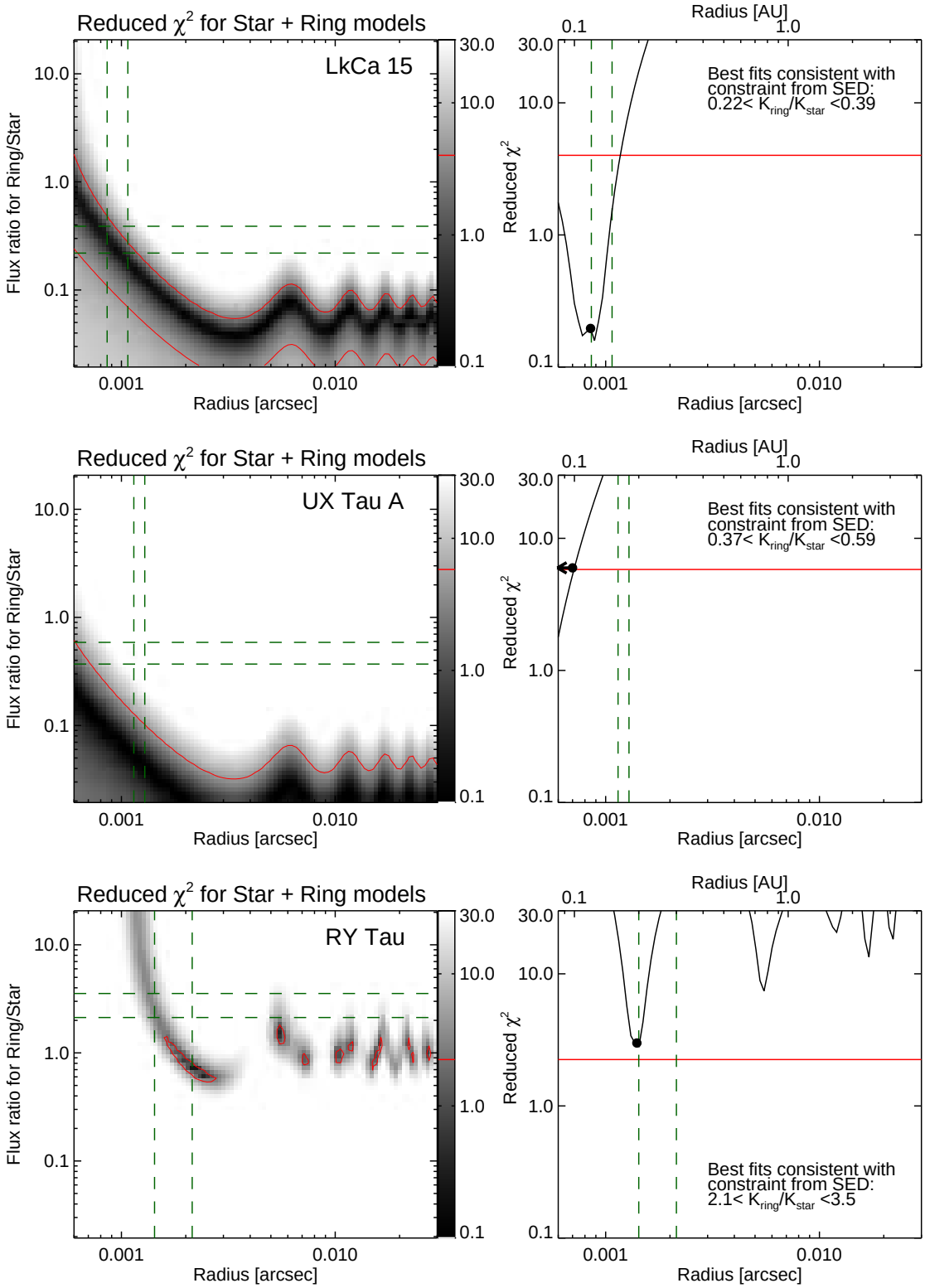

Fig. 4b.— Star plus ring fits to the interferometric data of LkHa 15, UX Tau A, and RY Tau. See caption to Figure 4a for a description of the plotted quantities.

spatially unresolved SED fits. The fact that there is very little 2 μm emission coming from the inner most disk region, might be due to low dust masses and an increased grain size.

Note that DM Tau is the only of the five targets which shows small sinusoidal wiggles in visibility across both hour angle, and varying baseline length (Fig. 2). Such wiggles might indicate a very close (near-contact) binary, with separation smaller than our 2 mas (= 0.3 AU) limit. Of course these wiggles are within the plotted measurement uncertainties. However, our conservative 3% errors mostly account for systematic visibility offsets from instrument setup to setup. Within a night and stable weather conditions the *relative* KI precision can be better, as is suggested also by our data reduction of the Dec. night (Sect.3). Dedicated calibration observations, close in space and time, would be needed to confirm such higher precision.

Such a close binary could not account for the large inner radius (3 AU) of the optically thick dust in DM Tau, unless very eccentric. Thus, this possibility was not discussed in Sect. 4.1. However, a close, equal-mass binary could mimic a single star in SED models that do not detect disk excess emission at near-infrared wavelengths. A recent study of transitional disks around accreting TTauri stars finds that only DM Tau does not show 5 μm veiling or circumstellar CO emission, which trace the dusty and gaseous disk components, respectively, although mass accretion has been detected (Salyk et al. 2009). A 1 mas, accreting binary (like DQ Tau, Boden et al. 2009) could be responsible for the apparent clearing of the innermost disk, on scales of 0.3 AU significantly inside the 3 AU inner radius of the outer optically thick disk. Follow-up time-resolved spectroscopy would be desirable.

4.3.2. GM Aur, expected $K_{\rm inner\,disk}/K_{\rm total}$: 12%

Calvet et al. (2005) fitted the same type of model to GM Aur as was used for DM Tau, using optically thin inner and optically thick outer dust. They find for GM Aur a dust disk distribution which is not completely devoid of inner dust: the inner, optically thin dust appears to not extend to radii larger then 5 AU, and the outer optically thick dust is outside of about 24 AU. Thus, they inferred a gap between the inner and outer dust distributions. With their given flux ratio, the KI data constrains the emission location of the bulk of the inner dust to be much further in, at radii of $\sim$ 1 mas, (0.15AU). Akeson et al. (2005b) report a slightly larger ring radius fitted to their single KI-data point (1.58 ± 0.6 mas), which is fully consistent with our findings due to our now increased u,v-coverage.

Due to the simplicity of the face-on ring model, the resulting radius is an order-of-magnitude estimation, but the resolution advantage of the interferometer over SED models

alone remains apparent. The visibility data constrains the location of the K-band excess emission significantly better. We did observe a significant trend of increasing visibilities with increasing hour angle and baseline length (Fig. 2). This could indicate that we observe an inclined disk, in which case our fit radius is a lower limit to the true radius. In particular, the published data point from (Akeson et al. 2005b) shows a *lower* visibility, i.e. a larger size, at a shorter baseline, i.e. at *lower* angular resolution. This cannot be explained with a circular-symmetric structure. Indeed,Simon et al. (2000) find with mm interferometry a disk inclination of 56 degrees for the cool outer disk around GM Aur. This (outer) disk inclination is confirmed by NICMOS images of scattered light (Schneider et al. 2003). The circular ring model hits with a disk inclination of 60 ° a validity limit. Higher inclinations could lead to a significant under estimation of the disk size, if modeled by a circular ring, but our sample does not include stars with disk inclinations beyond this limit.

Our limited *u,v*-coverage does not allow us to reliably fit an inclined disk / ring model, but a combined mm/NIR modeling approach might be worthwhile. Note, however, the following caveats: the inner hot disk might have a different orientation than the cool outer disk, and it is also possible that we observe a very close binary system instead of an inner disk, outside the fit range of Sect. 4.1.

4.3.3. LkCa 15, expected $K_{\mathrm{inner\,disk}}/K_{\mathrm{total}}$*: 23%*

Although its visibilities are lower than for GM Aur, we fit a smaller ring radius of about 0.7 mas to the data of LkCa 15, due to the larger flux contribution of the inner disk. Simon et al. (2000) fit similar inclination and position angles to the cool mm-disk of LkCa 15 and GM Aur. Given the increased disk dominance, a trend of the visibility versus hour angle should be stronger in LkCa 15, if the orientation angles are comparable. However, we do not observe such a trend within our uncertainties, which might be due to a combination of the interpretation caveats given in the previous section.

Based on near infrared spectroscopy, Espaillat et al. (2008) found that LkCa 15 has a gap between inner and outer optically thick dust, placing it as a member of the so-called "pre-transitional" disks. Such SED-models suggest that LkCa 15's optically thick inner disk is located between 0.12 and 0.15 AU (Espaillat et al. 2007b, 2008). Our high angular resolution data support these findings by confining the bulk of the inner dust radiation to within 1 mas (0.15 AU) from the star. Indeed, our best-fit ring radius is 0.85 ± 0.05 mas = 0.12 ± 0.01 AU. Note that the fact that our radius is slightly below the SED model estimation might be due to modelling an inclined inner disk (Table 1) with a face-on ring.

4.3.4. UX Tau A, expected $K_{\rm inner\,disk}/K_{\rm total}$: 32%

UX Tau A's properties, as measured by the KI, differ from our other targets. It is less spatially resolved. In fact the data are marginally consistent with a point source. Also, the Spitzer IRS spectrum shows a significantly weaker 10 μm silicate emission feature than in any other transitional disk. Both properties are surprising at first glance given the relatively large inner disk contribution as derived from SED models. The proposed explanation is an optically thick inner disk containing primarily large dust grains (Espaillat et al. 2007b). Those authors find characteristic radii for UX Tau A's optically thick inner and outer disks of 0.16 AU and 56 AU respectively. At the given flux ratio, our modeling suggests a ring radius smaller than 0.7 mas (0.1 AU) for a face-on disk. This roughly agrees with the numbers from the SED models, given the order-of-magnitude quality of our face-on ring models. In particular, the radius solutions of our circular ring model are likely slightly too small due the 60 ° inclination of the system (Espaillat et al. 2007b).

4.3.5. RY Tau, expected $K_{\rm inner\,disk}/K_{\rm total}$: 73%

In RY Tau, the NIR excess over the photospheric radiation is much more prominent than in the other targets. This is likely related to RY Tau's earlier spectral type, and thus hotter photosphere. The higher luminosity likely causes a puffed-up inner disk rim and increased NIR excess. Its visibilities are much lower than any other target (mean $V^2 = 0.28$), confirming that in the K band, this system's light is dominated by the extended disk. For RY Tau we took only three new KI data points, and added them to the measurements of an earlier PTI experiment (Akeson et al. 2005a). The availability of several baselines leads to the complete exclusion of the entire binary parameter range probed, as discussed in Sect. 4.1, assuming that the brightness distribution did not change significantly during the few years between the PTI observations and our KI experiment.

For the sake of comparison, we show in Fig. 4b our simple star plus face-on ring fit to the data, which shows the same two qualitative features as bnefore: the diagonal feature at low separation and the horizontal feature at larger separations–marking the resolved and over-resolved ring radii. The face-on ring model fits the data fairly well, although due to the much greater number of baselines probed, the reduced χ^2 significance limit is much reduced compared to our other targets, and no models for $K_{\rm inner\,disk}/K_{\rm total}$=73% fit within our 99.7% confidence level. This most likely suggests that we have moved beyond the applicability of our simplistic face-on ring model. Due to the addition of the PTI baselines, we are sensitive to the inclination of RY Tau, and we are consistent with the findings of (Akeson et al. 2005a), who found an inclination of 25 ± 3 degrees for a ring model. Our inferred ring radius

of ~ 1.5 mas agrees with the earlier findings within the uncertainties. Note that Muzerolle et al. (2003) reports a spectro-photometric model fit for RY Tau with a high disk inclination, which is not supported by the interferometric data (see the discussion in Akeson et al. 2005a). This demonstrates the need for high angular resolution.

4.4. Comparison with CoKu Tau/4

Recent high-resolution aperture-masking by Ireland & Kraus (2008) has revealed that the supposedly transitional disk around CoKu Tau/4 is instead a circumbinary disk around a near-equal flux binary with a (projected) star-star separation of 53 mas. Thus, there is no need to invoke planet formation to produce its inferred disk clearing within ~ 10 AU. But for all other known and well-studied transitional disks in Taurus, we have probed the binary separation range that could be responsible for creating the inner holes implied by the target SEDs, and concluded that the interferometric data rule out binarity as the predominant cause for the lack of hot dust emission in these systems. CoKu Tau/4 appears to be the exception, not the rule.

Is there any systematic difference between CoKu Tau/4 and other transitional disks which might let us distinguish between these two classes of objects based on other criteria? As previously noted by Ireland & Kraus (2008), one of the main differences is that only CoKu Tau/4 is a weak-lined TTS: its spectrum does not show significant signs of mass accretion (D'Alessio et al. 2005). However all five targets of our sample are mass-accreting classical TT stars, with typical accretion rates of $10^{-9..-8}\,M_\odot\,yr^{-1}$ (Calvet et al. 2005). This matches with the theoretical work of Artymowicz & Lubow (1994, and references therein), which suggests that accretion of a circum-binary disk onto the central stars is inhibited by the resonant torques at the circumbinary dust disk inner edge. Thus, the binary in the CoKu Tau/4 system may be the cause not only of the large disk hole, but also for the insignifcant accretion of the disk material onto the stars. Furthermore, our data confirm the presence of hot dust in the inner regions of the other transitional disks in our sample. This suggests a scenario in which true transitional disks will in general retain some small amount of hot, radiating dust inside of the outer, partially cleared optically thick disk. They also will have signs of accretion onto the central star. AU-scale binaries, however, may clear disks in a way that they mimic transitional disk SEDs, but lack ongoing accretion of material on sub-AU scales, inside the binary, and inside the outer optically thick dust, cleared by dynamical interaction with the binary.

5. Conclusions

The angular resolution of the Keck interferometer improves on single telescope adaptive optics imaging and aperture mask interferometery by about an order of magnitude. Within a single night of repeated observations, our experiment was sensitive to close binaries with 2.5 - 30 mas separation and flux ratios down to 0.05. However, we were able to rule out nearly all possible binary companions within that parameter range. For four of our targets, we cannot entirely rule out all possible companions due to the fixed PSF structure resulting from our u,v-coverage, but we do exclude companions from some 98-99% of the FOV. Observations along an orthogonal baseline (e.g. from CHARA or VLTI) should suffice to completely rule out the remaining part of parameter space, as was the case for RY Tau. Still, it is very unlikely that 4/5 of our targets would have hidden binaries aligned with the Keck interferometer's baseline at the time of the observation. Therefore, we conclude that binarity is not in general responsible for clearing disk holes to produce transitional-disk-type SEDs.

We spatially resolve a fraction of the K-band emission in all five stars, ranging between $\sim 4 - 70\%$ of the total K-band flux. By fitting a toy disk model to the data, we find that this inner disk emission comes from radii of about 1 mas (0.15 AU), consistent with previous work. In particular, these findings are consistent with disk models fitting spatially unresolved spectro-photometric data of transitional disks. A next step for studying transition disks at high angular resolution could be to fit more realistic models simultaneously to the observed visibilities and the SED, as has been recently done for a few systems (Tannirkulam et al. 2008, Pinte et al. 2008).

We confirm that the transitional disk phase is characterized by several distinct dust zones: an inner (of order 0.1 AU), and an outer part (of order $>$ 10 AU) which are not smoothly connected by a continuous distribtion of optically thick material. This supports the general hypothesis that these young objects are indeed in a transitional evolutionary state between primordial optically thick disks and optically thin disks. In each of our targets, the habitable zones are devoid of optically thick dust emission. The fact that we resolve excess emission very close to the star in a transitional disk, which lacks such emission further out, underlines that the evolution of a primordial disk is not as simple as a clearing from the inside out due to photoevaporation. In fact, the presence of gaps suggests that we may see the effect of planet formation on disks.

We are grateful to the team at WMKO and NExScI for making these observations a success. We thank R. Akeson for providing the reduced data of the previously published PTI and KI measurements of some of our sources. The data presented herein were obtained at the W.M. Keck Observatory, which is operated as a scientific partnership among the

California Institute of Technology, the University of California and the National Aeronautics and Space Administration. The Observatory was made possible by the generous financial support of the W.M. Keck Foundation. The authors wish to recognize and acknowledge the very significant cultural role and reverence that the summit of Mauna Kea has always had within the indigenous Hawaiian community. We are most fortunate to have the opportunity to conduct observations from this mountain. The Keck Interferometer is funded by the National Aeronautics and Space Administration as part of its Navigator program. This work has made use of services produced by the NASA Exoplanet Science Institute at the California Institute of Technology. This research has made use of the SIMBAD database, operated at CDS, Strasbourg, France.

Facilities: Keck:I (), Keck:II ()

REFERENCES

Akeson, R. L., et al. 2005a, ApJ, 622, 440

Akeson, R. L., et al. 2005b, ApJ, 635, 1173

Espaillat, C., et al. 2007a, ApJ, 664, L111

Espaillat, C., Calvet, N., D'Alessio, P., Hernández, J., Qi, C., Hartmann, L., Furlan, E., & Watson, D. M. 2007b, ApJ, 670, L135

Espaillat, C., Calvet, N., Luhman, K. L., Muzerolle, J., & D'Alessio, P. 2008, ApJ, 682, L125

Sicilia-Aguilar, A., et al. 2006, ApJ, 638, 897

Dullemond, C. P., & Dominik, C. 2005, A&A, 434, 971

van Boekel, R., et al. 2004, Nature, 432, 479

Boss, A. P., Wetherill, G. W., & Haghighipour, N. 2002, Icarus, 156, 291

Clarke, C. J., Gendrin, A., & Sotomayor, M. 2001, MNRAS, 328, 485

Skrutskie, M. F., Dutkevitch, D., Strom, S. E., Edwards, S., Strom, K. M., & Shure, M. A. 1990, AJ, 99, 1187

Stassun, K. G., Mathieu, R. D., Vrba, F. J., Mazeh, T., & Henden, A. 2001, AJ, 121, 1003

D'Alessio, P., et al. 2005, ApJ, 621, 461

Calvet, N., et al. 2005, ApJ, 630, L185

McCabe, C., Ghez, A. M., Prato, L., Duchêne, G., Fisher, R. S., & Telesco, C. 2006, ApJ, 636, 932

Furlan, E., et al. 2006, ApJS, 165, 568

Lada, C. J., et al. 2006, AJ, 131, 1574

Muzerolle, J., et al. 2006, ApJ, 643, 1003

Piétu, V., Dutrey, A., Guilloteau, S., Chapillon, E., & Pety, J. 2006, A&A, 460, L43

Simon, M., Dutrey, A., & Guilloteau, S. 2000, ApJ, 545, 1034

Ghez, A. M., Neugebauer, G., & Matthews, K. 1993, AJ, 106, 2005

Ghez, A. M., McCarthy, D. W., Patience, J. L., & Beck, T. L. 1997, ApJ, 481, 378

Leinert, C., Zinnecker, H., Weitzel, N., Christou, J., Ridgway, S. T., Jameson, R., Haas, M., & Lenzen, R. 1993, A&A, 278, 129

Simon, M., et al. 1995, ApJ, 443, 625

Duchêne, G., Ghez, A. M., McCabe, C., & Weinberger, A. J. 2003, ApJ, 592, 288

Artymowicz, P., & Lubow, S. H. 1994, ApJ, 421, 651

Melo, C. H. F. 2003, A&A, 410, 269

Ireland, M. J., & Kraus, A. L. 2008, ApJ, 678, L59

Mathieu, H. D. 1992, IAU Colloq. 135: Complementary Approaches to Double and Multiple Star Research, 32, 30

Flaherty, K. M., & Muzerolle, J. 2008, AJ, 135, 966

Brown, J. M., et al. 2007, ApJ, 664, L107

Brown, J. M., Blake, G. A., Qi, C., Dullemond, C. P., & Wilner, D. J. 2008, ApJ, 675, L109

Salyk, C., Blake, G. A., Boogert, A. C. A., & Brown, J. M. 2009, ApJ, 699, 330

Pinte, C., Ménard, F., Berger, J. P., Benisty, M., & Malbet, F. 2008, ApJ, 673, L63

Mora, A., et al. 2001, A&A, 378, 116

Muzerolle, J., Calvet, N., Hartmann, L., & D'Alessio, P. 2003, ApJ, 597, L149

Bertout, C., Robichon, N., & Arenou, F. 1999, A&A, 352, 574

Herbig, G. H., & Bell, K. R. 1988, Lick Observatory Bulletin, Santa Cruz: Lick Observatory, —c1988,

Cutri, R. M., et al. 2003, The IRSA 2MASS All-Sky Point Source Catalog, NASA/IPAC Infrared Science Archive. http://irsa.ipac.caltech.edu/applications/Gator/,

Schneider, G., Wood, K., Silverstone, M. D., Hines, D. C., Koerner, D. W., Whitney, B. A., Bjorkman, J. E., & Lowrance, P. J. 2003, AJ, 125, 1467

Calvet, N., Muzerolle, J., Briceño, C., Hernández, J., Hartmann, L., Saucedo, J. L., & Gordon, K. D. 2004, AJ, 128, 1294

Boden, A. F., Akeson, R. L., Sargent, A. I., Carpenter, J. M., Ciardi, D. R., Bary, J. S., & Skrutskie, M. F. 2009, ApJ, 696, L111

Palla, F., & Stahler, S. W. 1999, ApJ, 525, 772

Skrutskie, M. F., et al. 2006, AJ, 131, 1163

Meyer, M. R., Beckwith, S. V. W., Herbst, T. M., & Robberto, M. 1997, ApJ, 489, L173

Table 4: Derived binary limits and ring properties

	DM Tau	GM Aur	LkCa 15	UX Tau A	RY Tau
% FOV without companion > 0.05	96.0	94.8	97.7	94.3	100.
% FOV without companion > 0.1	99.8	99.6	99.9	98.7	100.
Best-fit ring radius ρ (mas)	> 1.5	1	0.85	< 0.7	1.4
Best-fit ring radius ρ (AU)	> 0.2	0.14	0.12	< 0.1	0.2
$\chi^2_{\rm red}$-limit (99.7 %)	3.6	4.6	4.0	5.8	2.2

Note. — The first two rows give the fraction of each field of view for which our data rule out the presence of any binary companions brighter than the stated flux ratio relative to the primary. The field-of-view probed is the annulus from 2.5 mas - 30 mas; inside of 2.5 mas our sensitivity rapidly degrades and some binary solutions with flux ratios near unity are allowed. The next two rows give the best-fit ring properties derived for face-on rings, assuming the K band flux excess for each target given in Table 1. The last row gives the 99.7 % χ^2 confidence levels for each dataset, which were used for rejecting model fits.